M. Abdolah Zadeh, A.M. Grande, S. Van Der Zwaag, S.J. Garcia
Effect of Curing on the Mechanical and Healing Behaviour of a Hybrid Dual Network: a Time Resolved Evaluation
RSC Advances, Vol. 6, N. 94, 2016, p. 91806-91814
doi:10.1039/C6RA17799A

Effect of curing on the mechanical and healing behaviour of a hybrid dual network: a time resolved evaluation

M. Abdolah Zadeh, A. M. Grande, S. van der Zwaag and S. J. Garcia*

Novel Aerospace Materials Group, Faculty of Aerospace Engineering, Delft University of Technology, Kluyverweg 1, 2629 HS, Delft, The Netherlands.

Abstract

In the present work we show the effect of the crosslinking degree on the mechanical and healing behaviour of a healable thermoset dual-network polymer. A hyphenated rheological test (i.e. simultaneous rheology and FTIR) was used to follow the effect of the curing process on the mechanical behaviour in relation to the underlying chemical reactions. The effect of curing on the bulk properties and the polymer interfacial healing was studied using gap closure kinetics and a fracture mechanical test. The increased crosslinking density at longer curing times led to a more temperature-stable polymer network with significantly higher mechanical properties (elastic modulus and strength at break). It was found that the damage closure kinetics decrease with the curing degree but the ultimate interfacial healing efficiency does not. The results here reported highlight the effect of the crosslinking density on the kinetics of damage closure with a low impact on the maximum interfacial healing efficiency as long as the amount of reversible bonds remains constant.

Introduction

Intrinsically healable polymers based on reversible chemistries have attracted considerable interest in the last few years due to their capability to undergo repeated healing.[1] Amongst the covalent reversible moieties disulphide bridges appear as one of the most versatile ones.[2] The pioneering work of Tobolsky et al.[3,4] demonstrated the significant effect of disulphide bonds on the viscoelastic behaviour of different polymers such as polyethylene[5] and polyurethane[6] already in the 40 s. Nevertheless, it was not until the 60 s that disulphide interchange was clearly proposed as the mechanism responsible for the stress-relaxation of such oligo-sulphide based polymers.[7,8]

As a result of the dynamic nature of the covalent disulphide (S–S) bonds, disulphide-based polymers exhibit good mechanical properties as well as efficient healing performance using a wide range of stimuli. Various triggering agents such as temperature,[9–11] shear forces,[2] reduction reactions[12,13] or UV-irradiation[14,15] can lead to selective scission of S–S bonds and on-demand flow of the polymeric networks. The selective opening of disulphide bridges can be facilitated and accelerated by the presence of nucleophilic reagents such as phosphine[16] and thiol groups.[17,18] In this later case the S–S bridge scission occurs via thiol-di/oligo-sulphide exchange reaction. Nevertheless, in has been reported that unfavourable oxidation of thiol groups can reduce the overall healing kinetics.[11,18] Additionally, the nature of the groups directly connected to the disulphide bridges also affects the kinetics of the disulphide bridge opening.[19] Furthermore, lower bond strengths and therefore higher bond interchange rates can be achieved by replacing disulphide bonds with tetrasulphides.[6–8]

Recently we introduced a healable hybrid thermoset dual network with dynamic di/tetra-sulphide bridges.[11] The thermos-reversible di/tetrasulphide bridges enabled thermo-mechanically induced

flow of the crosslinked networks while the irreversible organic and inorganic crosslinks preserved the mechanical integrity of the polymer during the healing process. This dual network showed remarkable macroscale damage closure capabilities (gap closure kinetics and final network restoration) at an optimal healing temperature of 70 °C.[11]

A part from the reversible moiety used, the healing performance of polymers is strongly affected by the polymer chemistry and architecture, e.g. content of the reversible bonds, crosslinking density, chain stiffness and intra-molecular interactions.[20–23] Moreover, the overall properties of the healed interface (e.g. mechanical, barrier) highly depend on the newly formed polymer architecture at the healed site (i.e. scar). A good understanding and evaluation of the healed zone and its long-term performance is of paramount importance for the ultimate industrial implementation of this new class of materials and is therefore attracting increasing attention.

Standard tensile tests are usually employed to evaluate the healing performance of polymers.[24,25] Although, the tensile procedure fails to distinguish the different processes taking place at the interface and can lead to overestimated values in terms of healing efficiency its value as a fast evaluation and screening tool is un-doubtful.[26] However, methods sensitive to discontinuities, such as fracture mechanics,[27] can potentially lead to a better understanding of the phenomena involved during the healing process and can provide more realistic values of the obtained healing degrees.[28,29] In the case of self-healing polymers with elasto-plastic behaviour (such as the dual network presented in our previous work[11]) accurate quantification of the fracture toughness is feasible using a fracture mechanics protocol based on the *J*-integral evaluation.[30]

In this work we analyse the effect of curing time on the time-resolved behaviour of a healable hybrid dual network polymer and its impact on mechanical, viscoelastic and healing properties. Rheological measurements were performed to evaluate the time/frequency dependent properties of the polymer through the application of the well-known time–temperature superposition (TTS) principle.[31] The effect of curing time was followed by monitoring the evolution of the dynamic shear moduli at different temperatures. Furthermore, to investigate the effect of curing time on the polymer bulk properties and its interfacial healing performance, flow and fracture tests were carried out on the polymer cured for 2 and 48 h. It was found that long curing times lead to a more stable polymeric network with improved mechanical properties and reduced flow kinetics. However, the maximum interfacial healing efficiency was found to be independent of the curing degree. Such behaviour is attributed to a completion of the inorganic crosslinking of the alkoxysilanes leading to an increase in the network stiffness but not affecting the availability of the reversible S–S bridges responsible for efficient interfacial healing.

Experimental

Materials

Epoxy resin based on Epikote™ 828 (184–190 g eq.$^{-1}$) and Ancamine®2500 curing agent (105–110 g eq.$^{-1}$) were provided by Akzo Nobel Aerospace Coatings (ANAC) and used as received. (3-Aminopropyl)trimethoxysilane (97%, M_W = 179.29 g mol^{-1}) and pentaerythritol tetrakis(3-mercaptopropionate) (>95%, M_W = 488.66 g mol^{-1}), hereon called APS and tetra-thiol respectively, were purchased from Sigma-Aldrich (the Netherlands) and used without further purification. Bis[3-(triethoxysilyl)propyl]tetrasulphide (99%, M_W = 538.95 g mol^{-1}, total sulphur content > 20%), hereon BS, was purchased from Capture Chemicals, China and used as received.

Polymer preparation

The polymers were prepared as described elsewhere.[11] The organically modified silicone alkoxides (OMSAs) were sequentially added (APS followed by BS) to the epoxy resin with an OMSAs : epoxy resin weight ratio of 1 : 1, keeping BS : APS molar ratio at 3 : 1. The mixture was stirred using a

magnetic stirrer at 300 rpm for 3 h at room temperature. The organic crosslinker (Ancamine®2500) was then added to the mixture keeping the amine hydrogen equivalent (AHE) to epoxy equivalent (EE) ratio at 1.1 and the mixture was stirred in a high speed mixer at 2500 rpm for 5 min. Tetra-thiol was then added in a tetra-thiol : epoxy resin weight ratio 0.56 : 1 to overcome phase separation problems and to facilitate cleavage of tetrasulfides via thiol-oligosulfide exchange reactions. Although it is expected that tetra-thiol will also participate in crosslinking reactions with epoxy, the network complexity and lack of secondary amine signal in FTIR did not allow for a exact quantification of its contribution in each of the possible roles. The mixture was further mixed in the high speed mixer for 40 s at 2500 rpm. The resulting mixture was casted in a PTFE mould to obtain polymeric films of 80 × 25 × 2 mm and subsequently was cured for either 2 or 48 h at 70 °C in an air circulated oven resulting in polymers with T_g of about 24 °C.[11,32]

Characterization

Dynamic thermo-mechanical analysis (DMTA). Dynamic mechanical thermal analysis (DMTA) measurements with in situ FTIR were performed using a Haake Mars III, Thermofisher rheometer coupled with Nicolet iS10 FTIR spectrometer. Circular samples of 20 mm diameter were tested in oscillatory shear mode using parallel-plate geometry.

For the TTS analysis storage (G') and loss (G'') shear moduli were measured as a function of temperature, frequency and time. A shear strain amplitude of 0.5% was employed to stay in the linear viscoelastic range of the hybrid polymer. The frequency sweep scans were performed in the range of 0.1–10 Hz at different temperatures from 25 °C to 70 °C with a temperature step of ΔT = 5 °C. Storage (G') and loss (G'') modulus master curves were then generated applying the time temperature superposition principle (TTS).

The effect of curing time was studied by measuring the dynamic shear modulus at a frequency of 1 Hz at seven different temperatures in the range of 50–110 °C with a step of 10 °C. The evolution of the dynamic shear modulus was followed for at least 2 hours at each of the testing temperatures. Simultaneous rheological and FTIR data were collected at every 10 minutes during the experiment. The time-resolved evolution of Si–O–Si bonds was followed by monitoring the changes in peak intensity of its characteristic resonance ($\upsilon_{Si-o-Si}$ = 1036 cm^{-1}).

Raman spectroscopy. Raman spectroscopy tests were performed using a U1000-high resolution double spectrometer from HORIBA Jobin Yvon with acquisition time of 1 min on a measurement spot of 1 mm diameter. The spectral region from 445 to 3260 cm^{-1} was collected using a laser with an excitation line of 632 nm at room temperature.

Gap closure kinetics test. To quantify the thermo-mechanical induced flow of the polymer leading to gap closure, hybrid sol–gel films of 15 × 4 mm were cut in two pieces at room temperature. The cut pieces were placed in parallel 500 ± 20 μm apart from each other between two glass plates under a constant pressure of 30 kPa. The ability of the polymer to close the artificial gap was investigated at 70 °C in an air circulation oven based on the optimal healing conditions reported elsewhere.[11] The gap size evolution was monitored with a Leica DMLM microscope in transmission mode and images captured with inbuilt Axio Cam ICc 3 digital camera. AxioVision software was employed for the analysis of micrographs and gap area quantification. Assuming a uniform thickness of the samples, the gap closure efficiency was calculated using the following equation:

$$\text{Gap closure efficiency}(\%) = \left(\frac{A_0 - A_t}{A_0}\right) \times 100 \quad (1)$$

where A_t and A_0 represent the gap area between the cut pieces at time (t) and (0), respectively.

Tensile testing. The tensile mechanical properties of the prepared films were evaluated at room temperature using a Zwick 1455 tensile testing machine. The dog-bone shaped samples (ASTM D1708) were tested in tension with a 1 kN load cell, a cross-head speed of 10 mm min^{-1}.

Fracture testing. To evaluate the effect of the curing time on the degree of interfacial strength recovery achieved during the healing process, double edge notched tension (DENT) tests were performed at room temperature on pristine and healed samples. DENT specimens were prepared by casting the hybrid polymers in a mould of 45 × 25 × 2 mm. Two 10 mm long notch was made in the middle of the specimen edge using a sharp razor blade. The samples were tested using a Zwick 1455 tensile testing machine equipped with a 1 kN load cell, a cross-head speed of 10 mm min^{-1} and a gauge length of 25 mm. The tested samples were then placed in a Teflon mould designed to correctly align the two crack planes. The mould with the sample was placed in an air circulation oven at 70 °C for a given time (2 h) based on previously published results.[11] The healed samples were subsequently notched at the previously damaged sites and tested using the same methodology. All experiments were recorded with a camera in order to detect the crack initiation and propagation.[28]

Results and discussion

Effect of curing time and temperature on the polymer network

The storage (G') and loss (G'') moduli master curves for the hybrid sol–gel polymer after 2 and 48 h curing time are shown in Fig. 1. Both polymers showed a relaxation process at low frequencies (increase of G''). Due to the chemical composition of the studied polymers this relaxation process can be attributed to the dynamic behaviour of polysulphide bridges.[29] The 48 h-cured polymer showed no increase of G' at high temperatures (Fig. 1a) indicating the presence of a stable network and the potential validity of the TTS principle. On the other hand, the oscillatory rheological measurements and subsequent preliminary application of the TTS principle to the 2 h-cured polymer showed a constant and gradual increase in the storage shear modulus (G') plateau at temperatures higher than 60 °C suggesting the presence of chemical reactions leading to an increase of the polymer crosslinking density. Due to this temperature effect on the polymer network the TTS approach was limited to up to 60 °C in the case of the 2 h cured polymer. The resulting shift factor (a_t) were fitted with an Arrhenius law (Fig. 1c):

$$\log(a_t) = \frac{E_a}{R}\left(\frac{1}{T} - \frac{1}{T_0}\right) \quad (2)$$

where E_a is the activation energy, R is the universal gas constant, and T_0 is a reference temperature (in this case 25 °C).

The fitting approach of the shift factors led to an activation energy (E_a) significantly higher for the 48 h-cured polymer (31.7 kcal mol^{-1}) than for the 2 h-cured one (19.1 kcal mol^{-1}), yet in general agreement with values reported in literature for polysulfide containing rubbers.[4]

As Fig. 1 shows, 48 h curing time led to a polymer network with higher elastic (G') and loss (G'') moduli in all the frequency range compared to 2 h curing. Such a trend further suggests an increase in the crosslinking density with the curing time and implies a higher chain mobility potential for low cured samples (2 h curing time). As will be presented later on, these aspects having a direct impact on the network mobility play a critical role on the healing process.

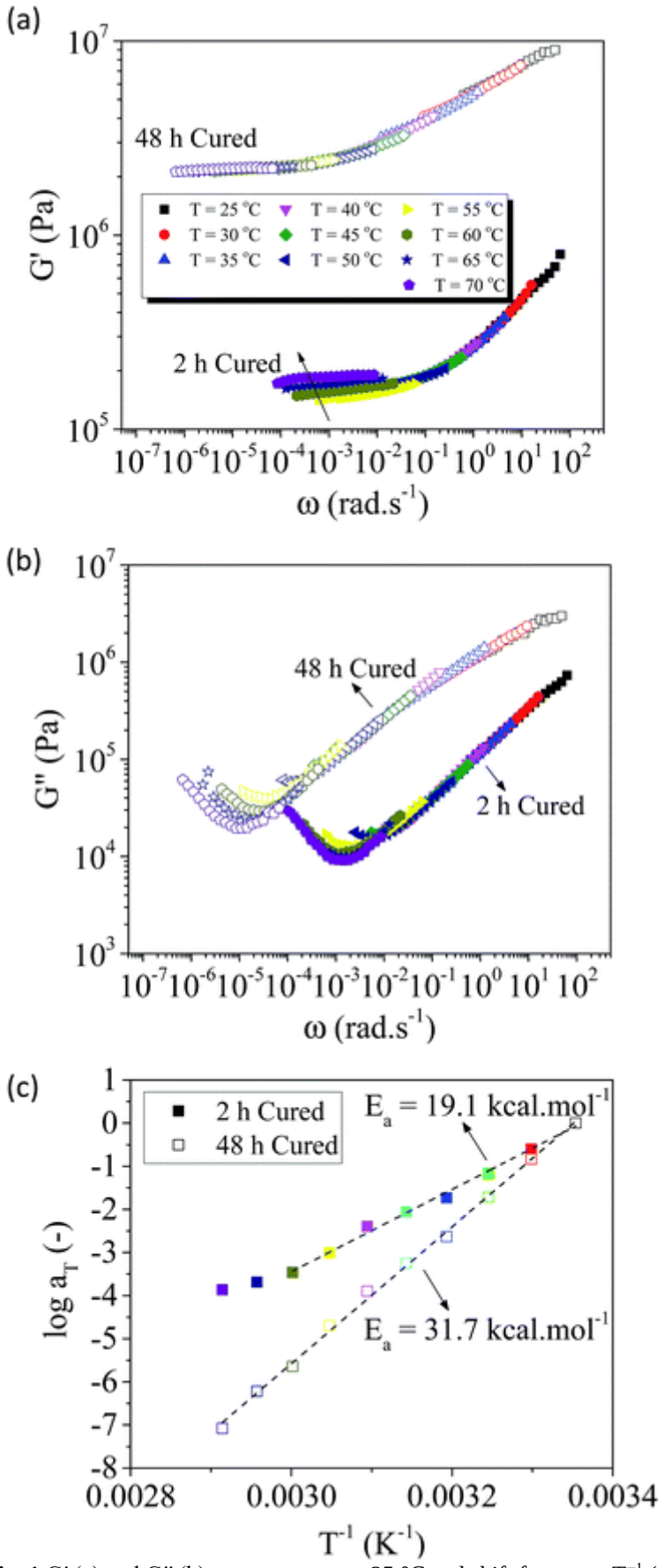

Fig. 1 G′ (a) and G″ (b) master curves at 25 °C and shift factor vs. T^{-1} (c).

In order to follow the evolution of the crosslinking processes and their effect on mechanical properties a hyphenated experimental procedure combining rheology and FTIR measurements was performed. From the mechanical point of view, time sweep scans illustrated a gradual increase of the storage modulus (*G′*) depending on the sample temperature during a curing time of 2 h (Fig. 2a). In particular, higher temperatures resulted in a more rapid growth of the storage modulus (*G′*) over the course of the measurements (e.g. 110 °C). As Fig. 2a shows, below 60 °C, there is no change in the storage modulus for the longest tested time (2 h). However, at temperatures higher than 60 °C, the storage modulus increased linearly without reaching a plateau on the time scale of 2 h. When defining the storage modulus growth rate as the slope of the different temperature curves in Fig. 2a, an exponential dependence on the curing temperature was obtained as shown in Fig. 2b. The observed *G′* evolution suggests the formation of new bonds stiffening the polymeric network.

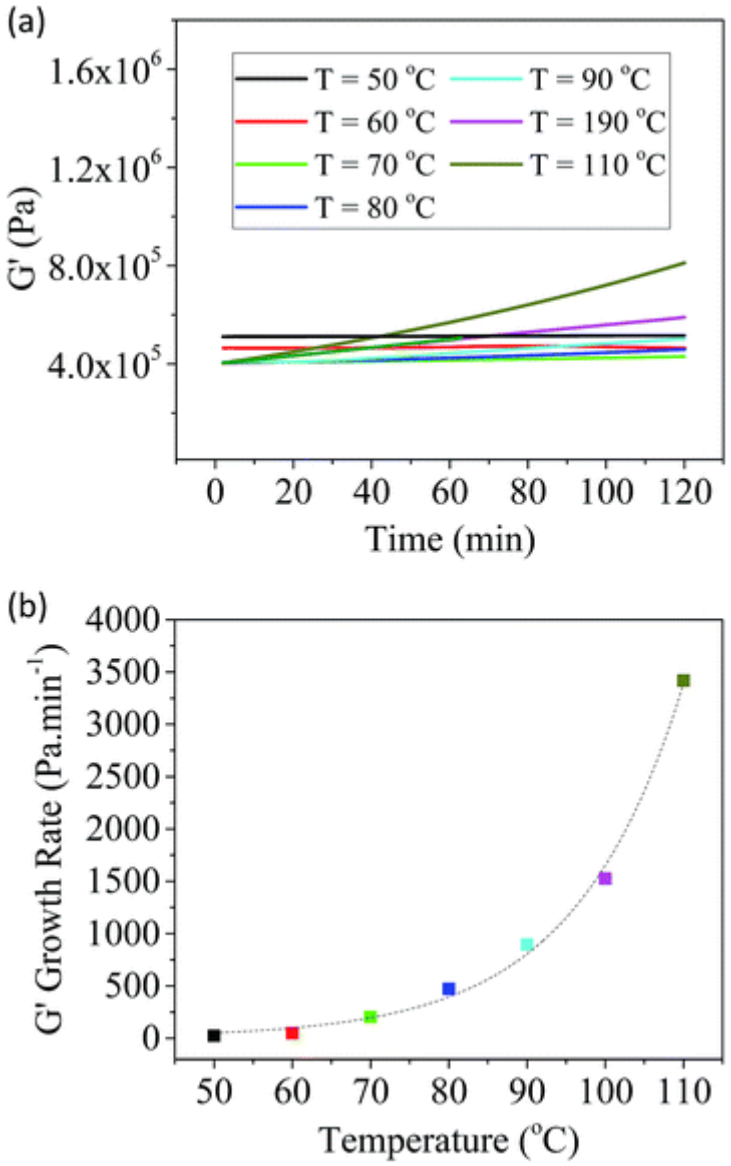

Fig. 2 Rheological time-sweep scans at 1 Hz and different temperatures (a) and the corresponding growth rate of the elastic modulus (G′) with temperature (b).

Fig. 3 shows the FTIR spectra of the polymer cured for 2 h and further cured at 100 °C for 120 minutes during a time sweep rheological scan. The FTIR spectra shows several characteristic bands in the spectral range of 4000–500 cm^{-1}; e.g. υ = 3450 cm^{-1} corresponding to O–H and N–H stretching, υ = 2968, 2925 and 2880 cm^{-1} associated with C–H stretching, υ = 1608 and 1450 cm^{-1} assigned to the aromatic ring stretching, υ = 1340 cm^{-1} associated with C–N stretching, υ = 1036 cm^{-1}

corresponding to Si–O–Si stretching and $\upsilon = 550\ cm^{-1}$ assigned to C–S stretching.[33] To get a better insight into the nature of chemical reactions proceeding during the second curing step, the FTIR spectra were studied in the whole spectral range. As Fig. 3b shows the peaks associated with the organic network (e.g. $\upsilon_{C=C-C} = 1450\ cm^{-1}$, $\upsilon_{C-N} = 1340\ cm^{-1}$ and $\upsilon_{C-S} = 550\ cm^{-1}$) exhibited no significant variations during the measurement. However, the characteristic peaks of the organically modified silicone alkoxides (OMSAs) i.e. $\upsilon_{Si-OH} = 956\ cm^{-1}$, $\upsilon_{Si-OC_2H_5} = 1075\ cm^{-1}$, $\upsilon_{Si-OCH_3} = 1100\ cm^{-1}$ and $\upsilon_{Si-O-Si} = 1036\ cm^{-1}$ varied considerably over 2 hours at 100 °C (Fig. 3c). While the intensity of the characteristic resonances of the $SiOCH_3$, $SiOC_2H_5$ and SiOH decreased, the one of the Si–O–Si significantly increased during the time sweep rheological scan (Fig. 3c). The variation of the aforementioned peak intensities can be explained by the following condensation reactions:[34]

$$\begin{aligned} &SiOR + H_2O \rightarrow SiOH + ROH \\ &SiOR + SiOH \rightarrow SiOSi + ROH \\ &SiOH + SiOH \rightarrow SiOSi + H_2O \end{aligned} \tag{3}$$

As eqn (3) illustrates, the condensation reactions of the alkoxy silanes (i.e. $SiOCH_3$ and $SiOC_2H_5$) and silanol groups (SiOH) result in formation of Si–O–Si bonds, justifying the descending trend in the peak intensities of the former groups and the ascending trend of Si–O–Si resonance in Fig. 3.
Using the C–H stretching band ($\upsilon_{C-H} = 2969\ cm^{-1}$) as the internal standard, the amount of $SiOCH_3$, $SiOC_2H_5$ and SiOH groups as well as Si–O–Si links at given times and temperatures were calculated using their normalized peak intensities based on eqn (4) and plotted in Fig. 4:

$$\text{Content of the groups} = I\left(\upsilon_{\text{group}}\right)_{T,t} \Big/ I\left(\upsilon_{C-H}\right)_{T,t} \tag{4}$$

Fig. 4 shows that at 50 and 60 °C the normalized peak intensities of the relevant groups did not vary significantly with time. Nevertheless at temperatures beyond 60 °C, the amount of $SiOCH_3$, $SiOC_2H_5$ and SiOH groups decreased linearly over the course of the measurements. Higher temperatures led to more rapid decay of the aforementioned groups. Such an effect was more pronounced at temperatures equal or higher than 100 °C due to a major solvent evaporation during the condensation of silanol and alkoxy silane groups (eqn (3)) and therefore condensation reactions. As a result of parallel phenomena taking place in the polymer during the post curing (e.g. chemical reactions and solvent evaporation), the process could not be modelled with a single Arrhenius process.
The observed decrease in the content of the alkoxy silane and silanol groups is associated with an increase in the content of the Si–O–Si bridges and therefore the crosslinking density of the inorganic network. In agreement with the rheological time sweep scans, the growth rate of the Si–O–Si links increased exponentially as a function of the testing temperature, manifesting the direct correlation between the content of newly formed irreversible bonds and the enhanced mechanical properties.

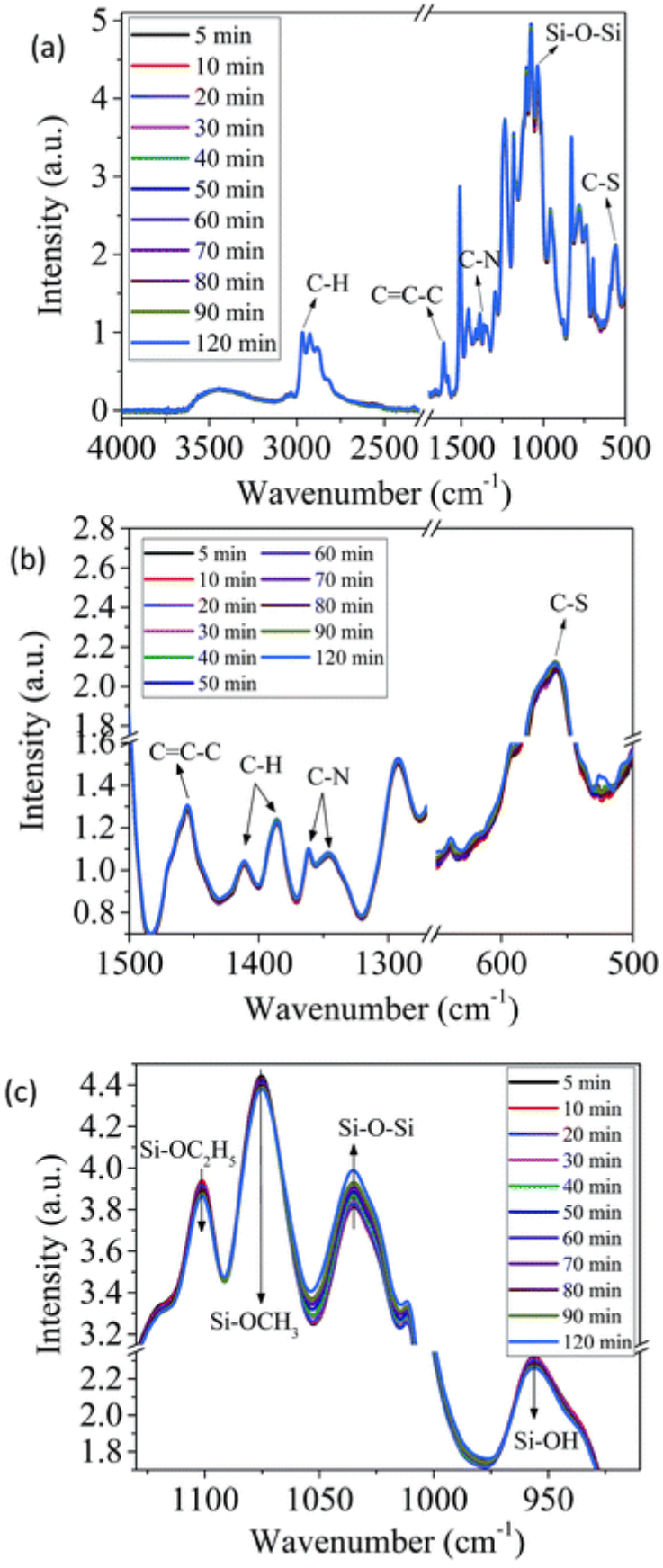

Fig. 3 FTIR spectra of the hybrid sol–gel polymer cured for 2 h and further cured at 100 °C during a time-sweep rheological scan: spectral range of 4000–500 cm^{-1} (a), 1500–500 cm^{-1} (b) and 1150–900 cm^{-1} (c).

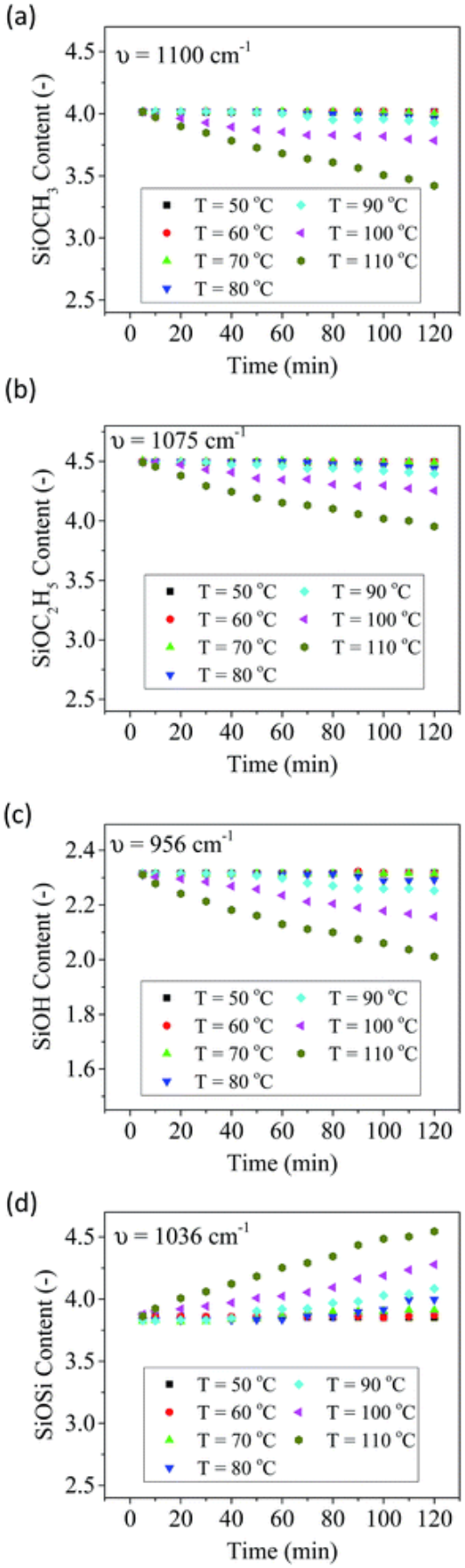

Fig. 4 Evolution of $SiOCH_3$ (a), $SiOC_2H_5$ (b), SiOH groups (c) and Si–O–Si bonds (d) of the hybrid sol–gel polymer cured for 2 h and further cured at different temperatures in a rheological time-sweep scan.

Fig. 5 shows the evolution of the storage modulus and the content of the Si–O–Si links in a 2 h-cured polymer during a post-curing step of 48 hours at 70 °C. As can be seen the storage modulus (*G′*) of the polymer increased exponentially over 48 hours, reaching a plateau at the end of the measurement. The amount of the Si–O–Si links calculated using the peak intensity criteria (eqn (4)) followed the same trend, further confirming the direct correlation between increased crosslinking density due to formation of the irreversible Si–O–Si bridges and the improved mechanical properties demonstrated by higher storage modulus values (*G′*). The obtained results further illustrate stabilization of the mechanical properties in the 48 h-cured hybrid sol–gel polymer thus not being affected by further temperature treatments.

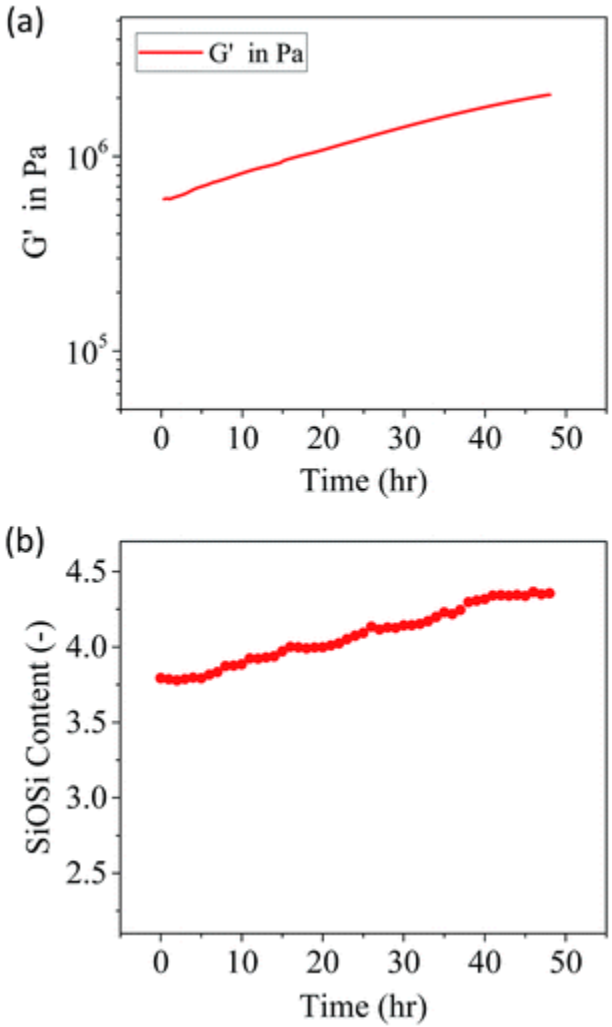

Fig. 5 Evolution of G′ (a) and content of Si–O–Si links (b) in a 2 h-cured hybrid sol–gel polymer during a rheological time-sweep scan performed at 70 °C.

Raman analysis (Fig. 6) also revealed the presence of free thiol groups in both 2 h and 48 h cured samples by presence of the characteristic resonance of S–H bonds (υ_{S-H} = 2570 cm^{-1}).[33] Furthermore, the characteristic resonance of S–S stretching (υ_{S-S} = 510 cm^{-1})[33] was chosen for the identification and qualitative quantification of S–S bonds in the two sets of samples. Using the C–C stretching band (υ_{C-C} = 1186 cm^{-1}) as the internal standard, the amount of S–S and S–H bonds at room temperature were calculated using the peak area ratio. While the amount of S–H groups was 3.8% lower after 48 h curing than after 2 h, the content of the S–S bridges was about 1.5% higher, suggesting the temperature triggered oxidation of free thiol groups to S–S in air.[11]

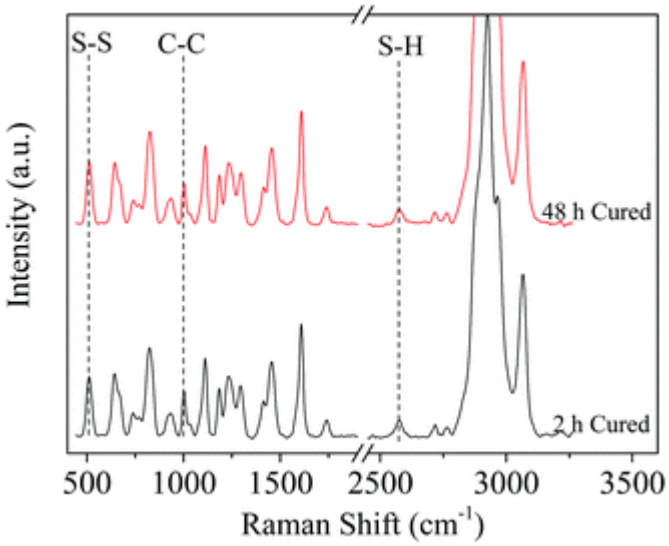

Fig. 6 Raman spectra of the hybrid polymer after 2 and 48 h curing time.

Effect of curing on tensile mechanical response, gap closure kinetics and interfacial healing

As previously anticipated the higher crosslinking density obtained at longer curing times may have a significant effect on the final polymer mechanical and healing behaviour. It is therefore important to evaluate the effect of the crosslinking degree on mechanical properties, gap closure kinetics and interfacial healing degree in order to progress towards the development of polymers combining high mechanical properties and healing behaviour (kinetics and final interfacial strength).
Fig. 7 shows that longer curing times (48 h) led to a yield stress of about three times higher than that of short curing times (2 h). Moreover a pronounced strain hardening behaviour (slope of the stress–strain curve after yielding) was observed in the high crosslinked polymer leading to three times higher strength at break. On the other hand, the mildly crosslinked polymer showed an extended plastic region (from ~2.5% strain up to the break point). All the observed aspects indicate a reduced flow tendency and a less ductile behaviour when the crosslinking is higher.[35]

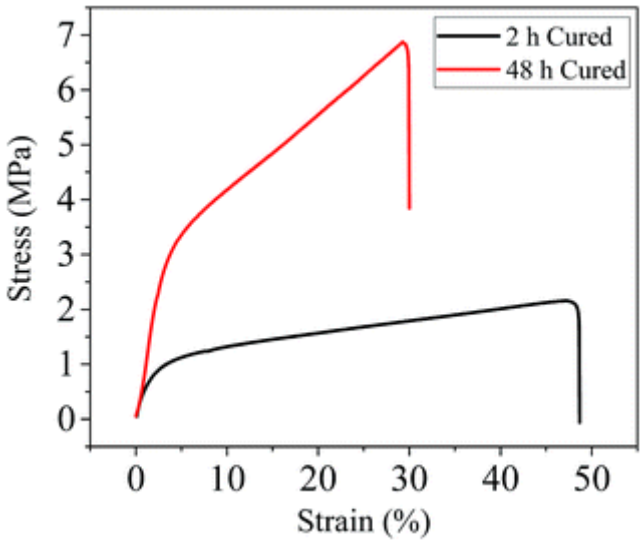

Fig. 7 Stress–strain plots of the fresh and post-cured hybrid sol–gel polymer

Fig. 8 shows the effect of the crosslinking density (2 h vs. 48 h at 70 °C) on the gap closure kinetics. The results clearly show reduced flow kinetics of the highly crosslinked polymer compared to the less crosslinked one. While the partially crosslinked sample is able to close a gap with an average

width of 500 μm in less than 5 min, the fully crosslinked one (48 h) took more than 20 min to cover and close a gap of the same dimension. These results are well in-line with previous mechanical and rheological measurements, where higher E_a was found for the highly crosslinked polymer. The lower gap closure kinetics of the highly crosslinked polymer can be attributed to the higher crosslinking density achieved by formation of new Si–O–Si bridges, as demonstrated in the FTIR studies. It is therefore clear that higher crosslinking reduces the gap closure kinetics.

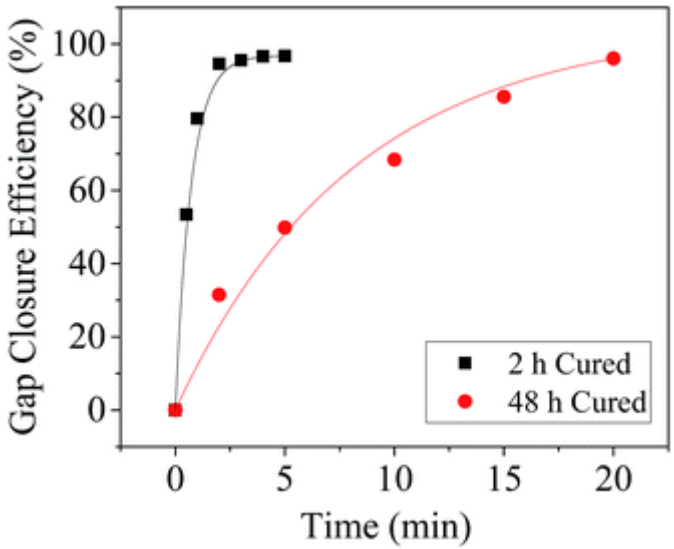

Fig. 8 Gap closure kinetics of the hybrid healing polymer 70 °C for 2 and 48 h

To evaluate the effect of crosslinking density on the interfacial healing performance of the hybrid sol–gel polymers a fracture mechanics based test protocol for ductile polymers was employed. Fracture experiments were performed on both 2 and 4 h-cured polymers.

The load–displacement curves for the virgin DENT samples and the ones healed at 70 °C for different times (10 min, 30 min, 1 h, 2 h, 4 h and 12 h) are presented in Fig. 9. As Fig. 9 shows, the 2 h-cured polymer showed lower mechanical properties than the 48 h-cured one. However, for both polymers, lower mechanical properties were exhibited by the healed DENT specimens compared to the virgin specimens. Additionally, a preliminary healing time dependent behaviour was detected for the two crosslinking degrees (2 h and 48 h).

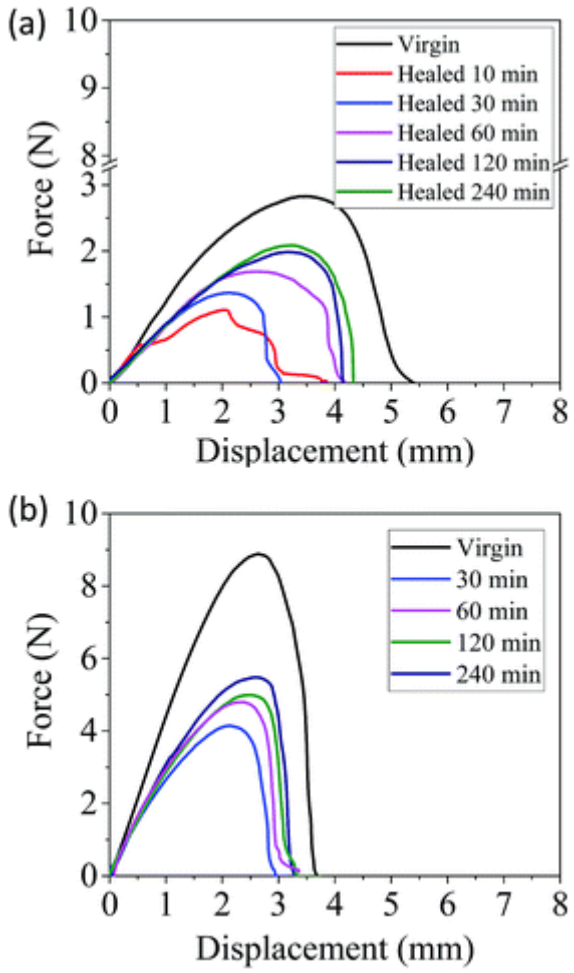

Fig. 9 Force–displacement plots of the virgin and healed DENT specimens for the 2 h-cured (a) and the 48 h-cured (b) hybrid sol–gel polymer

To estimate the material resistance to crack propagation, the critical *J*-integral value (J_{IC}) was selected as reference parameter.[28] Critical fracture energy values, J_{IC}, for each sample were calculated according to the following equation:

$$J_{IC}\left(\text{kJ m}^{-2}\right) = \left.\frac{U_c}{b(w-a)}\right|_{u_c} \tag{5}$$

where *b*, *w* and *a* are the sample thickness, sample width and pre-crack length, respectively and U_c is the energy calculated as the area under the load–displacement curves at the displacement u_c where crack starts to propagate. Crack initiation was detected by image analysis of the recorded video, as illustrated in Fig. 10.

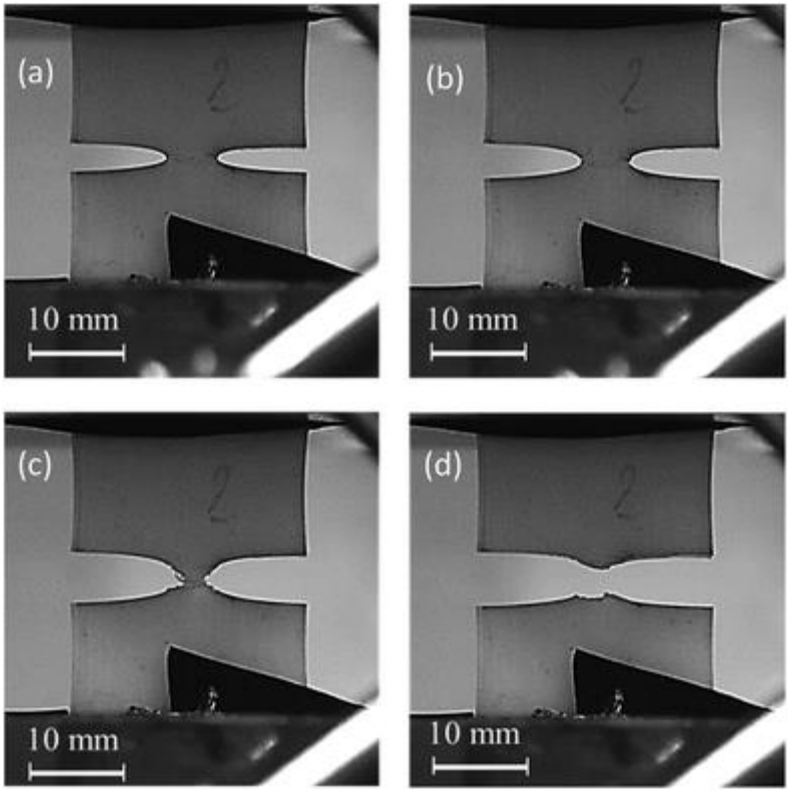

Fig. 10 Micrographs of the DENT specimen of the hybrid polymer after 2 h and 48 h curing time at 70 °C during the fracture test corresponding to loading (a), crack initiation (b), crack propagation (c) and failure (d).

The healing efficiency was calculated based on the following eqn:

$$\text{Healing efficiency}(\%) = \frac{J_{IC}^{healed}}{J_{IC}^{virgin}} \times 100 \quad (6)$$

where J^{healed}_{IC} and J^{virgin}_{IC} are the critical *J*-integral for healed and virgin samples, respectively.
The interfacial healing efficiency of the 2 h and 48 h-cured samples measured by fracture mechanics analysis are presented in Fig. 11. As Fig. 11 shows, the healing efficiency of the mildly crosslinked polymer (2 h) continuously increased with the healing time from about 20% reaching a plateau of 60% after 2 hours. The highly crosslinked polymer (48 h) exhibited a remarkably high recovery of the fracture property (around 45%) already at short healing times. Interestingly, for short healing times the healing efficiency of the fully crosslinked polymer was higher than that of the mildly crosslinked one. The surprisingly higher healing efficiency of the highly crosslinked polymer at short times can be explained by the higher interfacial wetting facilitated by the formation of a smoother surface during the fracture process due to the more brittle character of this polymer. The effect of surface wetting is also reported in literature[20,28] demonstrating its prominent influence on the kinetics of the healing process in polymeric materials. Interestingly, despite the differences in healing degrees at short healing times, both polymers showed a similar degree of healing at long healing times (t > 600 min) suggesting an equivalent extent of chain bridging at the fracture site.

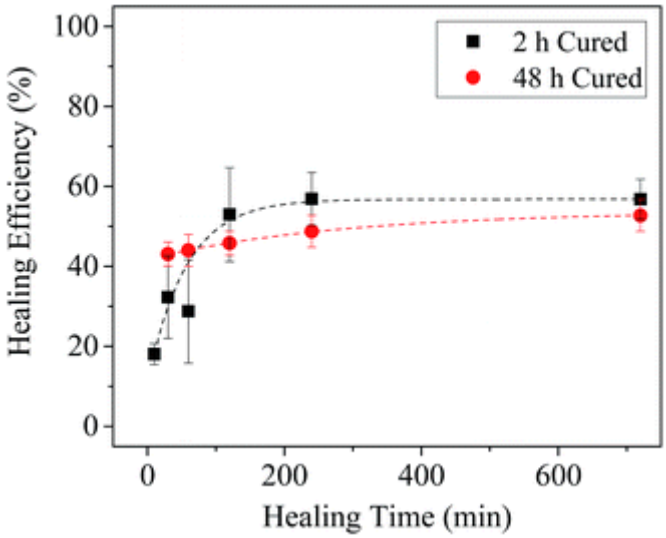

Fig. 11 Healing efficiencies of the 2 h and 48 h cured hybrid sol–gel polymers calculated based on J_{IC}

Based on the obtained results, it is possible to state that longer curing times of the hybrid sol–gel polymer increases the mechanical properties due to an increase in the crosslinking density. This affects the gap closure kinetics but does not affect the final overall healing behaviour. These results suggest that high crosslinking times do not directly affect the dynamics of the reversible bonds, although it clearly has an influence on the global viscoelastic behaviour of the material and on the morphology of the fracture surfaces thereby affecting the short term healing efficiency. It becomes thus clear that, while maintaining the same amount of reversible bonds, both fracture surface and the viscoelastic behaviour have a direct impact on the healing process (closure kinetics and final interface strength) since they both affect the capability of the material to flow and to promote an efficient contact between the fracture surfaces.

Conclusions

Several experimental procedures were adopted to evaluate the effect of the curing time on the mechanical and healing properties of a healable hybrid dual network polymer with disulphide bridges. A fracture mechanics protocol was introduced to assess the recovery of the interfacial properties. A hyphenated experimental procedure combining rheology and FTIR spectroscopy revealed an increase in the crosslinking density of the hybrid sol–gel polymer with the curing time due to the formation of additional Si–O–Si bonds. The increased crosslinking density during the long curing times yielded a higher flow activation energy (E_a) lowering the macroscopic flow kinetics (gap closure). Yet, the chemical species involved in the healing process were not significantly affected by the extra curing time. This fact combined with a smoother fracture surface led to equivalent healing efficiencies independently of the curing time although the more crosslinked polymer reached the maximum healing degree at an earlier stage.

Acknowledgements

The authors would like to acknowledge the Dutch National IOP program on self-healing materials for grant IOP-SHM-1028.

Notes and references

1. Y. Yang and M. W. Urban, Chem. Soc. Rev., 2013, 42, 7446–7467.

2. B. Gyarmati, Á. Némethy and A. Szilágyi, Eur. Polym. J., 2013, 49, 1268–1286.
3. M. D. Stern and A. V. Tobolsky, J. Chem. Phys., 1946, 14, 93–100.
4. M. Mochulsky and A. V. Tobolsky, Ind. Eng. Chem., 1948, 40, 2155–2163.
5. A. V. Tobolsky, R. B. Beevers and G. D. T. Owen, J. Colloid Sci., 1963, 18, 353–358.
6. G. D. T. Owen, W. J. MacKnight and A. V. Tobolsky, J. Phys. Chem., 1964, 68, 784–786.
7. A. Tobolsky, W. MacKnight and M. Takahashi, J. Phys. Chem., 1964, 68, 787–790.
8. A. Tobolsky, W. MacKnight and M. Takahashi, Rubber Chem. Technol., 1966, 39, 524–529.
9. J. Canadell, H. Goossens and B. Klumperman, Macromolecules, 2011, 44, 2536–2541.
10. U. Lafont, H. van Zeijl and S. van der Zwaag, ACS Appl. Mater. Interfaces, 2012, 4, 6280–6288.
11. M. AbdolahZadeh, C. Esteves, A. Catarina, S. Zwaag and S. J. Garcia, J. Polym. Sci., Part A: Polym. Chem., 2014, 52, 1953–1961.
12. J. Kamada, K. Koynov, C. Corten, A. Juhari, J. A. Yoon, M. W. Urban, A. C. Balazs and K. Matyjaszewski, Macromolecules, 2010, 43, 4133–4139.
13. J. A. Yoon, J. Kamada, K. Koynov, J. Mohin, R. Nicolaÿ, Y. Zhang, A. C. Balazs, T. Kowalewski and K. Matyjaszewski, Macromolecules, 2012, 45, 142–149.
14. H. Otsuka, S. Nagano, Y. Kobashi, T. Maeda and A. Takahara, Chem. Commun., 2010, 46, 1150–1152.
15. B. D. Fairbanks, S. P. Singh, C. N. Bowman and K. S. Anseth, Macromolecules, 2011, 44, 2444–2450.
16. R. Caraballo, M. Rahm, P. Vongvilai, T. Brinck and O. Ramstrom, Chem. Commun., 2008, 6603–6605.
17. T. Oku, Y. Furusho and T. Takata, Angew. Chem., Int. Ed., 2004, 43, 966–969.
18. M. Pepels, I. Filot, B. Klumperman and H. Goossens, Polym. Chem., 2013, 4, 4955–4965.
19. J. M. Matxain, J. M. Asua and F. Ruiperez, Phys. Chem. Chem. Phys., 2016, 18, 1758–1770.
20. R. P. Wool and K. M. O'Connor, J. Appl. Phys., 1981, 52, 5953–5963.
21. Y. H. Kim and R. P. Wool, Macromolecules, 1983, 16, 1115–1120.
22. S. J. Garcia, Eur. Polym. J., 2014, 53, 118–125.
23. T. Ge, M. O. Robbins, D. Perahia and G. S. Grest, Phys. Rev. E: Stat., Nonlinear, Soft Matter Phys., 2014, 90, 012602.
24. P. Cordier, F. Tournilhac, C. Soulie-Ziakovic and L. Leibler, Nature, 2008, 451, 977–980.
25. A. Rekondo, R. Martin, A. Ruiz de Luzuriaga, G. Cabanero, H. J. Grande and I. Odriozola, Mater. Horiz., 2014, 1, 237–240.
26. S. Bode, M. Enke, M. Hernandez, R. K. Bose, A. M. Grande, S. van der Zwaag, U. S. Schubert, S. J. Garcia and M. D. Hager, Journal, 2016, 273, 113–142.
27. C. Creton and M. Ciccotti, Rep. Prog. Phys., 2016, 79, 046601.
28. A. M. Grande, S. J. Garcia and S. van der Zwaag, Polymer, 2015, 56, 435–442.
29. A. M. Grande, J. C. Bijleveld, S. J. Garcia and S. van der Zwaag, Polymer, 2016, 96, 26–34.
30. J. M. Hodgkinson and J. G. Williams, J. Mater. Sci., 1981, 16, 50–56.
31. J. D. Ferry, Viscoelastic properties of polymers, John Wiley & Sons, 1980.
32. M. Abdolah Zadeh, S. van der Zwaag and S. J. Garcia, ACS Appl. Mater. Interfaces, 2016, 8, 4126–4136.
33. P. Larkin, in Infrared and Raman spectroscopy; principles and spectral interpretation, Elsevier, 2011, ch. 6.
34. C. J. Brinker and G. W. Scherer, Sol–gel science: the physics and chemistry of sol–gel processing, Academic press, 2013
35. Y.-W. Mai and P. Powell, J. Polym. Sci., Part B: Polym. Phys., 1991, 29, 785–793